Microfossil assemblages (diatoms, calcareous nannofossils, and silicoflagellates), paleoenvironment, and hydrocarbon source rock potential of the Oligocene Ruslar Formation at Karadere, Bulgaria

Emilia TULAN[1],* , Reinhard F. SACHSENHOFER[1] , Jakub WITKOWSKI[2] ,
Gabor TARI[3] , Stjepan ĆORIĆ[4] , Achim BECHTEL[1]
[1]Montanuniversitaet Leoben, Leoben, Austria
[2]Institute of Marine and Environmental Sciences, University of Szczecin, Szczecin, Poland
[3]OMV Exploration & Production GmbH, Vienna, Austria
[4]Geological Survey of Austria, Vienna, Austria

Abstract: The Oligocene Ruslar Formation, an equivalent of the Maykop Suite, is a potential hydrocarbon source rock in the western Black Sea Basin. In contrast to the offshore areas, the depositional environment and hydrocarbon source rock potential of onshore Bulgaria sediments are largely unknown. Hence, a 14-m-thick section of the Ruslar Formation, exposed near Karadere (Black Cape) along the Black Sea coast, provides an excellent opportunity to study the upper part of the Ruslar Formation. Here, laminated diatom-rich mudstones with frequent thin sandstone beds and a prominent concretion horizon are exposed. Furthermore, the fossil diatom assemblages provide a key component to understand the paleoenvironment. Overall, Paleogene diatoms are understudied in the Black Sea Basin and therefore only a genus-level study is undertaken here. The studied Ruslar Formation contain remarkably diverse and well-preserved diatom assemblage with 23 different genera. The most frequent genera are *Paralia*, *Distephanosira*, and *Stephanopyxis*. Common genera include *Coscinodiscus*, *Hemiaulus*, *Pseudopodosira*, *Rouxia*, and *Xanthiopyxis*. Rare taxa include *Actinoptychus*, *Asterolampra*, *Azpeitia*, *Delphineis*, *Distephanosira*, *Diploneis*, *Eunotogramma*, *Eurossia*, *Lyrella*, *Liradiscus*, *Plagiogramma*, *Radialiplicata*, *Rutilaria*, *Saeptifera*, and *Triceratium*. The diatom assemblages together with calcareous nannoplankton, silicoflagellates, and the presence of rare foraminifera indicate a fully marine neritic environment without major salinity variations. The calcareous nannoplankton investigated can be assigned to biozone NP23 (Early Oligocene). The exposed fragment of the Ruslar Formation was deposited after the low salinity "Solenovian event", which represents the maximum isolation of the Paratethys present in the lower part of the NP23. Bulk geochemical parameters from 35 samples (avg. TOC: 1.80% wt.; avg. HI: 226 mg HC/g TOC) show that the exposed part of the Ruslar Formation contains type II-III kerogen and a fair to good hydrocarbon potential. The Ruslar Formation is immature (avg. Tmax: 424 °C), but may generate about 0.5 tons of hydrocarbons per square meter if mature. Biomarker proxies support the low maturity and are characterized by diatom-related biomarkers (24-norcholestane; C_{25} HBI alkanes and thiophenes). Land-plant-derived biomarkers suggest a significant input of angiosperms. Based on biomarker ratios, the depositional environment was oxygen-depleted but probably not strictly anoxic. Reworking of biomass by chemoautotrophic bacteria is suggested by the presence of 28,30-bisnorhopane.

Key words: Black Sea, Oligocene, Ruslar Formation, hydrocarbon source rock, diatom assemblages, calcareous nannofossils

1. Introduction

Oligocene and Lower Miocene (Maykopian) pelitic rocks are considered important source rocks in the Black Sea area (Sachsenhofer et al., 2018a, 2018b; Mayer et al., 2018b), but also contain sandstone beds, which may act as hydrocarbon reservoirs (e.g., Tari and Simmons, 2018). In on- and offshore Bulgaria, the Oligocene rocks are termed the Ruslar Formation (e.g., Aladzova-Hrisceva, 1991). In offshore Bulgaria, the Ruslar Formation is cut by the deep shelf-break Kaliakra canyon filled with Oligocene

to Middle Miocene deposits including Lower Miocene diatom-rich sediments with a high petroleum potential (Mayer et al., 2018a; Sachsenhofer et al., 2018a, 2018b).

The thickness of the Oligocene Ruslar Formation is some tens of meters in onshore Bulgaria (e.g., Valchev et al., 2018) and increases to approximately 400 m on the western Black Sea shelf (Mayer et al., 2018a). In the West Black Sea Basin (WBSB), Oligocene to Lower Miocene Maykopian sediments are several kilometers thick (Sinclair, 1997; Georgiev, 2011; Nikishin et al., 2015).

* Correspondence: emilia.tulan@gmail.com

154

To date, only the Ruslar Formation on the western Black Sea shelf has been studied for its hydrocarbon potential (Sachsenhofer et al., 2009; Mayer et al., 2018a) using mainly cutting materials from exploration boreholes (see Figure 1 for well locations). Typically, the Ruslar Formation is represented by marls, shales, occasionally siltstone, sandstones, and limestones. Apart from the fill of the Kaliakra canyon, diatom-rich sediments have not yet been described within the Ruslar Formation of offshore Bulgaria.
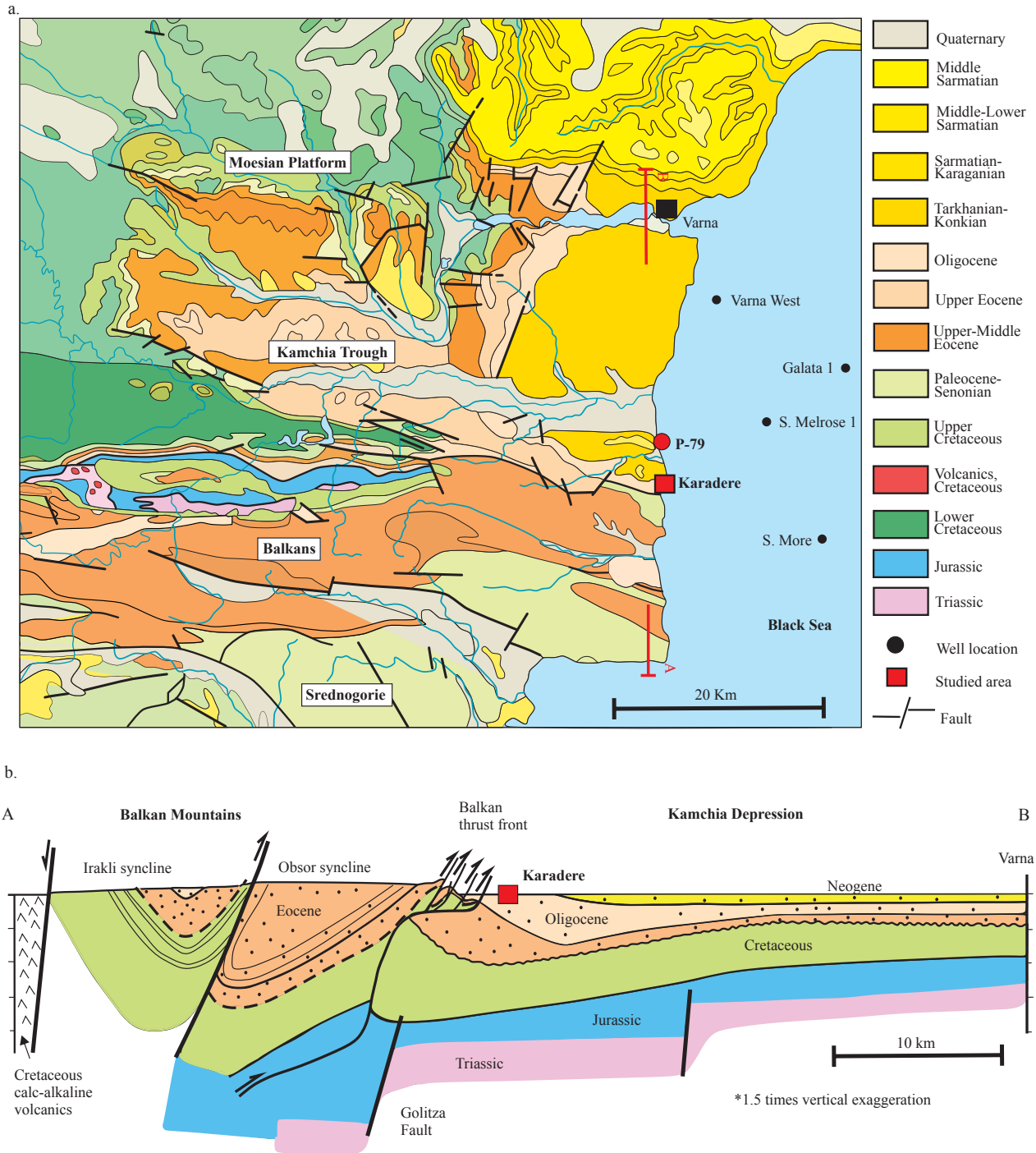

Figure 1. a) Geological map of eastern Bulgaria (after Cheshitev and Kancev, 1989) indicating the studied area and the position of the Bulgaria offshore wells; b) S-N cross-section through the Balkan Orogen and the Kamchia Depression along the Black Sea coast (after Sinclair et al., 1997), with the position of the studied area.

In order to enhance the knowledge of the westward extension of the Oligocene petroleum system, here we present a study of diatom-rich mudstones of the Ruslar Formation that crop out along the Bulgarian Black Sea coast near Karadere (Suttill, 2009; Figure 1). Neither their hydrocarbon potential nor their fossil diatom assemblages have been studied yet. The objectives of this study are to identify the hydrocarbon potential of the onshore Ruslar Formation, to document the siliceous microfossil and calcareous nannoplankton assemblages, and to contribute to the understanding of the depositional environment.

2. Geological setting
The Kamchia Depression, a foredeep basin, is located to the north of the Balkans thrust front in eastern Bulgaria (Figure 1) and continues offshore into the Black Sea (Sinclair et al., 1997; Georgiev, 2011). The sedimentary fill of the basin contains Middle Eocene to Quaternary deposits and is related to the growth of the Balkan mountain belt (Sinclair et al., 1997). Its base is marked by the intra-Middle Eocene Illyrian unconformity (Figure 2) (Georgiev, 2011). Another unconformity separates Eocene and Oligocene rocks (e.g., Mayer et al., 2018a).

The development of the Kamchia Basin began with the stacking of the Eastern Balkan thrust-belt during the Illyrian northward compression in the early Middle Eocene (Georgiev and Dabovski, 2001) and was controlled by the uplift of the Balkan thrust-fold belt and the opening of the WBSB (Georgiev, 2011). This Cenozoic basin is superimposed on the southern margin of the Moesian Platform and the frontal zone of the Balkan thrust-fold belt (Dachev et al., 1988). The Cenozoic sediments are preserved approximately 70 km inland from the coast of the Black Sea (Figure 1); thicker and younger sediments are present offshore (Sinclair et al., 1997).

The Oligocene Ruslar Formation overlies the Middle to Upper Eocene Avren Formation (~1.5 km thick; sandy marls with limestone and sandstone intercalations) with a major erosional unconformity and underlies the Middle Miocene Galata Formation (sandstones intercalated with frequent clays and rare limestone beds) (Popov and Kojumdjieva, 1987) (Figure 2).

The Ruslar Formation onshore (Valchev et al., 2018) and offshore Bulgaria (Sachsenhofer et al., 2009; Mayer et al., 2018a) typically contains from base to top calcareous shales (assigned to biozone NP21-22), marlstones to limestone (lower part of NP23), and overlying pelitic rocks with low carbonate contents (upper part of NP23 to NP24). In onshore Bulgaria, the base of the Ruslar Formation contains manganese ores and is sandier than offshore. The marlstones and limestones represent the low salinity "Solenovian event", when the Parathethys became isolated from the Tethys Ocean during the early part of
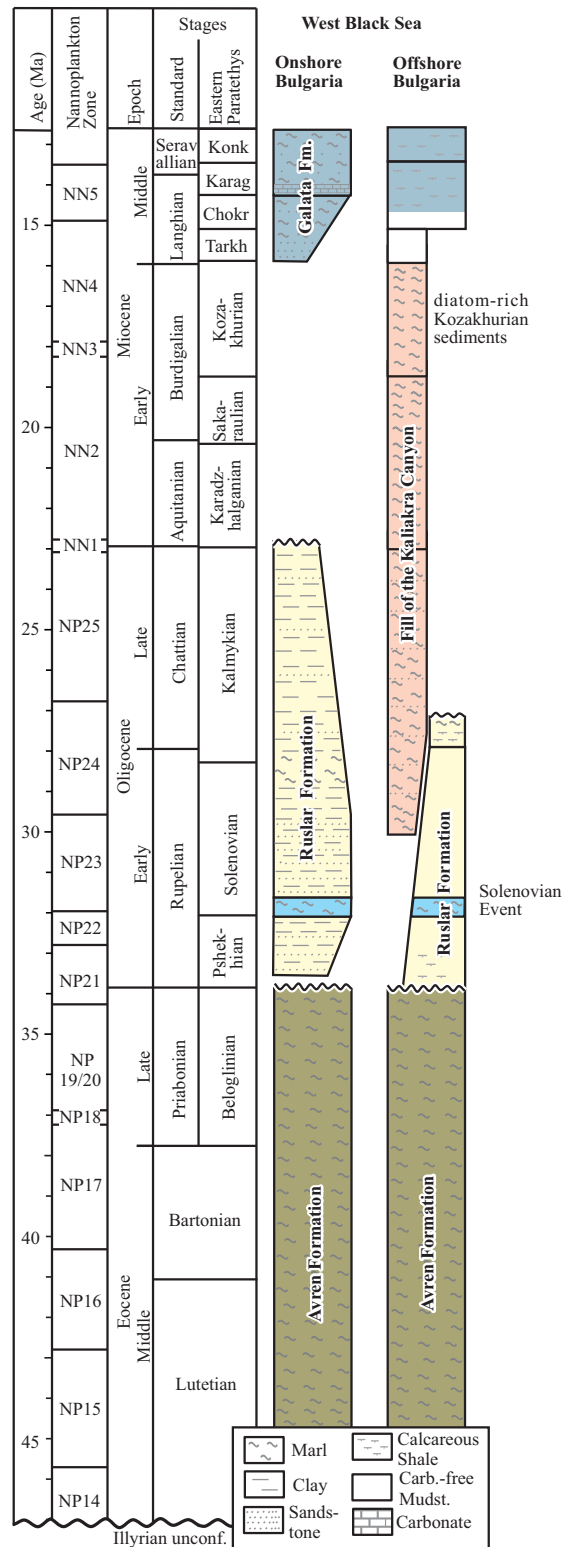

Figure 2. Stratigraphy of Middle Eocene to Middle Miocene sediments of onshore (mainly after Suttill, 2009 and Valchev et al., 2018) and offshore Bulgaria (after Sachsenhofer et al., 2018b). unconf. – unconformity; Carb.-free Mudst. – carbonate-free mudstone.

nannoplankton zone NP23 (Báldi, 1984; Voronina and Popov, 1984; Rögl, 1997; Rusu, 1999; Schulz et al., 2004). Later, the connection with the open ocean was partially restored during upper NP23 (Popov et al., 1993).

The thickness of the Ruslar Formation varies considerably, from some tens of meters north of Varna (Valchev et al., 2018) to ~70 m in the Varna area and ~400 m in the shelf sector of the Kamchia Basin (e.g., in the Samotino More well, for location see Figure 1; Sachsenhofer et al., 2009; Mayer et al., 2018a), and up to several kilometers in the WBSB (e.g., Nikishin et al., 2015).

In offshore Bulgaria, the Ruslar Formation is cut by a deep west-east-trending shelf-break canyon (the Kaliakra canyon), which developed during Lower Oligocene (Late Solenovian) time and which became filled with Oligocene to Middle Miocene deposits (Mayer et al., 2018a). Diatom-rich sediments occur in the Lower Miocene part of the canyon fill, which, although partly Oligocene in age, is not considered as part of the Ruslar Formation (Figure 2).

Near Karadere (known also as Black Cape), a part of the Ruslar Formation is exposed in 20-m-high cliffs on the Bulgarian Black Sea coast (Suttill, 2009).

3. Methods

A total of 29 fine-grained samples have been collected from the Ruslar Formation near Karadere with a sampling spacing of 50 cm. In addition, six cuttings samples from borehole P-72, which is located about 4 km north of Karadere (see Figure 1) and drilled the Ruslar Formation between 320 and 405 m in depth, were included in the study for comparison.

Total carbon (TC), total sulfur (S), and total organic carbon (TOC) contents were analyzed using an ELTRA elemental analyzer for all samples. Samples for TOC measurements were decarbonized with concentrated phosphoric acid. Results are given in weight percent (% wt.). Total inorganic carbon (TIC) was determined (TIC = TC – TOC) and used to calculate calcite equivalent percentages (TIC × 8.333; e.g., Schulz et al., 2004).

Pyrolysis measurements were performed for all samples using a Rock-Eval 6 instrument. The S1 and S2 peaks (mg HC/g rock) were used to calculate the petroleum potential (S1 + S2 [mg HC/g rock]), production index (PI = S1 / (S1 + S2) (Lafargue et al., 1998), and hydrogen index (HI = S2 / TOC × 100 [mg HC/g TOC]). Tmax was measured as a maturity indicator.

The mineral composition was determined for Karadere samples with a Bruker AXS D8 Advance X-ray diffraction (XRD) spectrometer (copper radiation generated at 40 kV and 40 mA). The powdered samples were placed carefully in sample holders to create a flat upper surface to achieve a random distribution of lattice orientation. Diffrac.Eva software was used according to the method of Schultz (1964).

Flame atomic absorption spectroscopy was performed on all samples to determine organic silica content using the methods described by Zolitschka (1988). Approximately 100 mg of sample material and 50 mL of 0.5 mol/L potassium hydroxide solution were boiled for 1 h to dissolve the opaline diatom valves. Afterwards, a 5-mL aliquot of the solution was diluted with distilled water (1:1). A PerkinElmer 3030 atomic absorption spectrometer was used for analysis and operated with a CH_4-N_2O flame to create free Si atoms in a gaseous state. A Si-hollow cathode lamp was used as a spectral line source. The AAS was calibrated using a Merck CertiPUR* silicon-standard solution (#1.1231.0500).

Eleven samples from the Karadere section were selected for biomarker analysis and extracted using dichloromethane in a Dionex ASE 350 accelerated solvent extractor at 75 °C and 50 bar. Afterwards, asphaltenes were precipitated with a hexane-dichloromethane solution (ratio 80:1 according to volume) and separated by centrifugation. Medium-pressure liquid chromatography using a Köhnen-Willsch instrument was used to separate the hexane-soluble fractions into NSO compounds, saturated hydrocarbons, and aromatic hydrocarbons (Radke et al., 1980).

The saturated and aromatic hydrocarbon fractions were analyzed by a gas chromatograph equipped with a 60-m DB-5MS fused silica column (i.e. 0.25 mm; film thickness 0.25 mm), coupled to a Thermo Fisher ISQ dual-quadrupole mass spectrometer. Using helium as a carrier gas, the oven temperature was programmed from 40 °C to 310 °C at 4 °C/min increase, followed by an isothermal period of 40 min. With the injector temperature at 275 °C, the samples were injected splitless. The spectrometer was operated in the electron ionization (EI) mode over a scan range from m/z 50 to 650 at 0.7 s of total scan time. Individual compounds were identified by retention time in the total ion current chromatogram and the comparison of the mass spectra with published data. Percentages and absolute concentrations of various compound groups in the saturated and aromatic hydrocarbon fractions were calculated using peak areas in the gas chromatograms and their relations to the internal standards (deuterated n-tetracosane and 1,1'-binaphthyl, respectively). Concentrations were normalized to TOC.

Smear slides for nannofossil identification were prepared from 10 Karadere samples using the standard preparation method described by Perch-Nielsen (1985). Nannofossil identifications were made using light microscopy (LM) and scanning electron microscopy (SEM). In LM, all samples were investigated under 1000× magnification with parallel and crossed nicols. Biostratigraphic assignments were made in accordance with the nannoplankton zonation of Martini (1971). For siliceous microfossil examination, 1 g of dry sediment from 11 samples was treated for 2 days with 30 mL of 33% hydrochloric acid (HCl) and 30 mL

of 33% hydrogen peroxide (H_2O_2) (Schrader, 1973). After the reaction settled, the solution was heated to 90 °C to finish the reaction. The samples were cooled and washed three times with 30 mL of distilled water. The solution was then sieved through a 50-µm sieve to concentrate the fine fraction. For microscope slides, 2 mL of solution was strewn on a glass slide. For the determination of the relative abundance of diatom genera, the first 300 valves were counted following the method of Schrader and Gersonde (1978). In addition to slides, thin sections were prepared from 10 samples. Nannofossil smear slides, siliceous microfossil slides, and thin sections were studied using a Leica DM 2500P microscope and pictures were taken with a Leica DFC490 camera. In addition, some of the diatom valves were examined and photographed using a scanning electron microscope.

4. Results

4.1. Lithology
Approximately 20-m-high cliffs of the Ruslar Formation are exposed along the Bulgarian Black Sea coast near Karadere (Black Cape; Figure 1). Neither the erosional base nor the top of the Ruslar Formation are exposed. However, large blocks with the coarse-grained Galata Formation at the northern end of the section indicate that the erosional surface at the base of the Miocene Galata Formation is very close, suggesting that the outcrop represents the upper part of the Ruslar Formation, which is reported to be about 70 m thick in the area.

The exposed part of the Ruslar Formation is dominated by laminated mudstones intercalated with sandstone layers and lenses. Sandy laminations are ubiquitous, but their frequency declines in the upper part between 11 m (sample 22) and 13 m (sample 26). At 11.5 m (between samples 23 and 24), a horizon with massive concretions is observed (Figures 3 and 4).

Based on the XRD analysis mudstones are composed on average of 57% clay minerals, 27% quartz, and 6% calcite. The percentages of dolomite, feldspar, ankerite, siderite, and pyrite do not exceed 2% (Figure 3).

Thin-section observations (Figure 5) indicate that organic matter-rich laminated argillaceous mudstone is the dominant lithology. The laminae are parallel, planar, and continuous. Sometimes sandstone laminae are seen.

Figure 3. Karadere (Black Cape) section with Ruslar Formation. a) Outcrop section from south; b) outcrop section from north; c) argillaceous mudstone alternating with sandstone laminations and sand lenses; d) concretions.
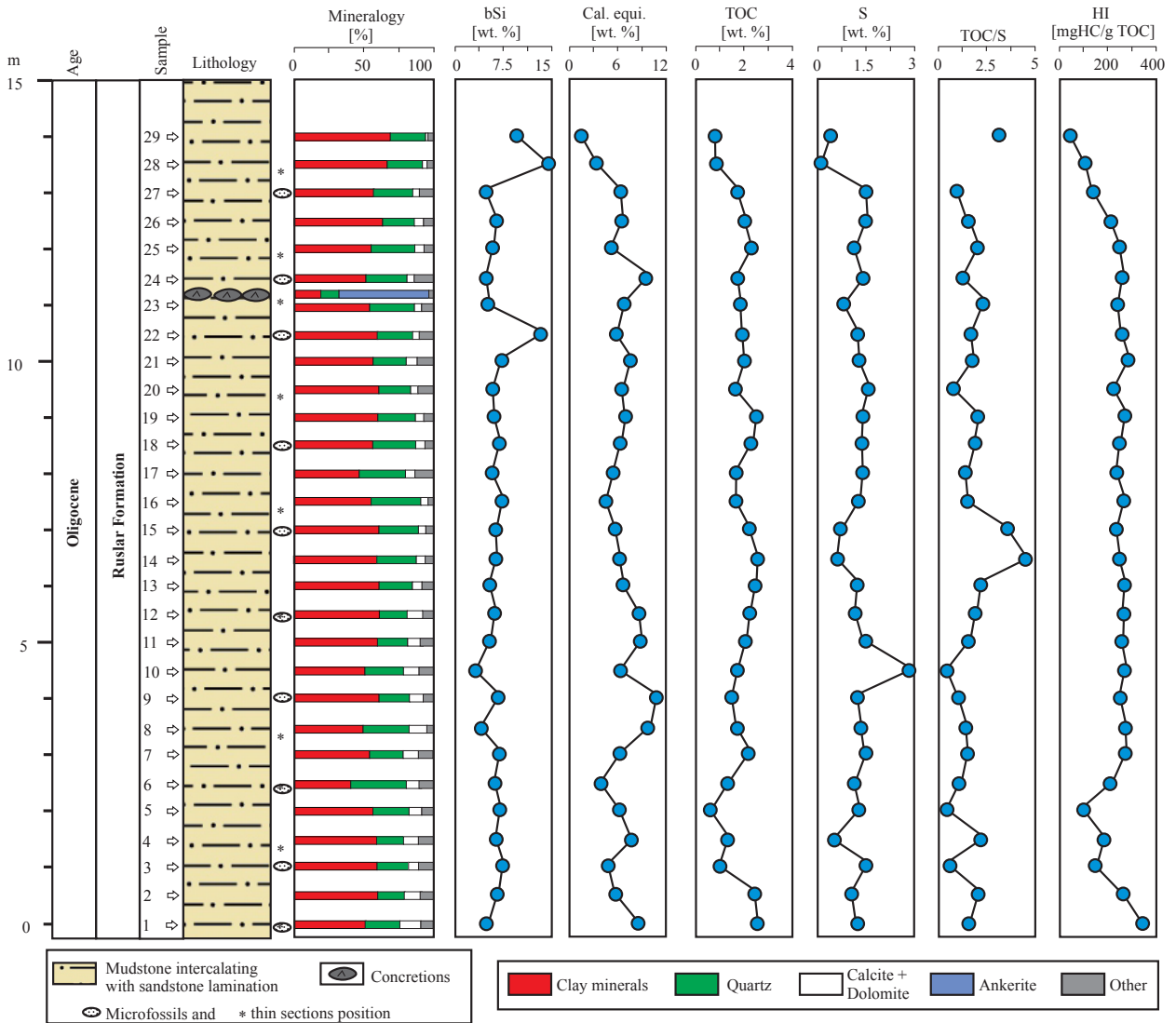
Figure 4. Bulk geochemical parameters and mineralogy of the Ruslar Formation beds exposed at Karadere. bSi - biogenic silica; Cal. equi. - calcite equivalent; TOC - total organic carbon; S - total sulfur; HI - hydrogen index; Other minerals: feldspar, pyrite ankerite, siderite.

Abundant diatom valves, well-sorted angular quartz with subordinate feldspar, glauconite, and (globigerinid) foraminifera are observed. In addition, the presence of intact diatom chains suggests that at the time of deposition the sediments were not disturbed.

Based on XRD, the concretions (Figure 3) contain about 60% ankerite. Detrital grains (angular quartz and feldspar) within the concretions form a few continuous parallel and planar layers. Diatom valves and foraminifera in concretions are very rare.

Biogenic silica (bSi) contents are on average 6.5% (Figure 3) and do not show a clear depth trend. Two samples have relatively high biogenic silica contents (sample 22: 13% bSi; sample 28: 14.6% bSi). Similar

biogenic silica contents (8.5%–13.0% bSi) were measured for cutting samples from the nearby borehole P-79.

4.2. Bulk parameters
Bulk parameters of the Ruslar Formation exposed at Karadere are plotted stratigraphically in Figure 4 and listed in Table 1. The average total organic carbon (TOC) content is 1.85% wt. TOC contents below 1.5% wt. are restricted to samples 3 to 5 (1.5–2.5 m) and 28 to 29 (14–14.5 m). Sulfur (S) contents typically follow the TOC trend except sample 10 (5.0 m), where S content is 2.90% wt. (avg. 1.25% wt.). TOC/S ratios on average are 1.94 and show an increase in the middle of the section (samples 14–15; 7–7.5 m) due to low S contents (sample 14: 0.56% wt.; sample 15: 0.60% wt.).
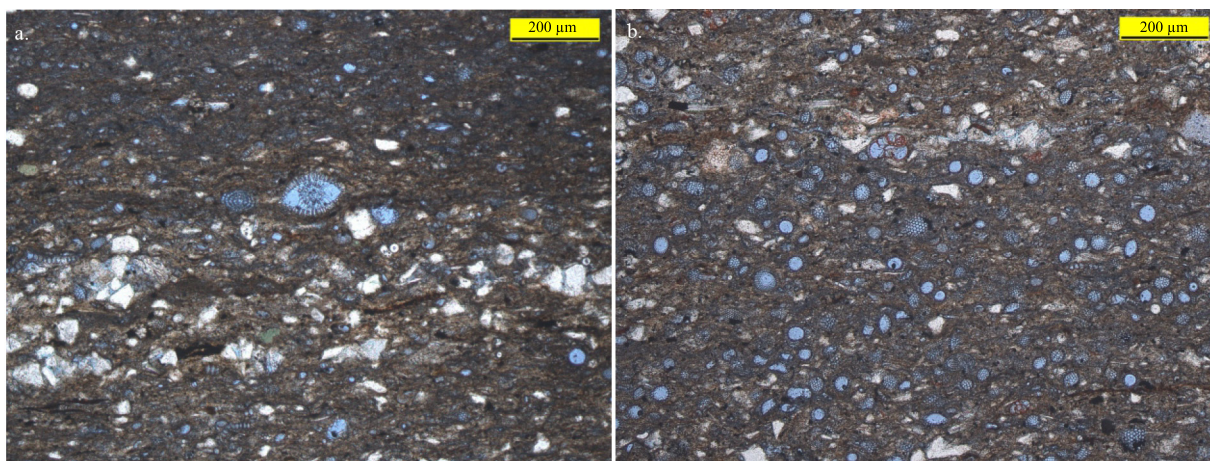
Figure 5. Selected thin-section photographs of Ruslar Formation exposed at Karadere. a) Organic matter-rich laminated argillaceous mudstone and angular quartz grains with common diatom valves (sample 6 - 3.0 m); b) diatom-rich argillaceous mudstone with rare detritus (sample 12 - 6.0 m).

S2 values reach a maximum of 8.48 mg HC/g rock (Figure 6) (avg. 4.51 mg HC/g rock) and the HI values range from 61 to 331 HC/g TOC, indicating the presence of type II–III kerogen. Tmax varies between 421 and 436 °C.

TOC and Rock-Eval data from cuttings samples from well P-79 (350–410 m depth; for location see Figure 1) are listed in Table 1. The average TOC content is 1.77% wt. Sulfur contents are on average 1.08% wt. and TOC/S ratios vary between 1.35 and 1.94. S2 values are on average 2.71 mg HC/g rock, reaching a maximum of 4.65 mg HC/g rock (400 m). HI values are between 102 and 206 HC/g TOC. According to the plot of HI versus Tmax, the Ruslar Formation in P-72 is immature and contains predominantly type III kerogen (Figure 6).

4.3. Biomarker data
Biomarker data have been determined for 11 samples from the Ruslar Formation at Karadere. The extractable organic matter (EOM) yields of the Ruslar Formation vary between 8.99 and 39.0 mg/g TOC and are dominated by polar NSO-compounds (62%–76% of EOM; Table 2). In contrast, saturated and aromatic hydrocarbons are very rare. Consequently, only some biomarker ratios could be determined (Table 2).

4.3.1. n-Alkanes and isoprenoids
The saturated hydrocarbons are dominated by long-chain n-alkanes (n-C_{27-31}: avg. 45%), which are characteristic for higher land plants (mainly plant waxes; Eglinton and Hamilton, 1967) and short chain n-alkanes, typically related to algae and microorganisms (n-C_{15-20}: avg. 30%). The middle chain n-alkanes are present as well (n-C_{21-25}: avg. 25%), which may originate from aquatic macrophytes (Ficken et al., 2000).

Concentrations of pristane (Pr) and phytane (Ph) are variable with height. Pr/Ph ratios of <1 may indicate

anoxic conditions, while ratios between 1 and 3 indicate dysoxic conditions (Didyk et al., 1978). The calculated Pr/Ph ratios (0.67–1.29) may indicate oxygen-depleted and partly anoxic conditions. The low maturity of the section (avg. Tmax: 424 °C) can affect the Pr/Ph ratios; therefore, the values should be treated with caution.

4.3.2. Steroids
The concentration of steroids has a high range (2.1–64.1 µg/g TOC). Sterenes, the immature precursors of steranes, are dominated by C_{29} sterenes (38%–69%), whereas C_{27} sterenes (14%–36%) and C_{28} sterenes (16%–26%) are detected in low amounts.

4.3.3. Terpenoids
Hopanes are nonaromatic cyclic triterpenoids that originate from precursors in bacterial membranes (Ourisson et al., 1979). Their concentration in the Ruslar Formation ranges from 0.8 to 6.5 µg/g TOC. High steroids/hopanoids ratios (3.0–9.9) reflect a strong predominance of eukaryotic (e.g., algal) over bacterial biomass (Moldowan and Fago, 1986).

The presence of hop-17(21)-ene (0.04–1.17 µg/g TOC) supports the low maturity of the samples (Ten Haven, 1985). According to Bechtel et al. (2002, 2004, 2007), the biological source of hop-17(21)-enes can be related to anaerobic bacteria.

28,30-Bisnorhopane is present in the Ruslar Formation with relative high concentrations (avg.: 19.4 µg/g TOC). This compound has been suggested to indicate reworking of organic matter by chemoautotrophic bacteria (Noble et al., 1985; Watson et al., 2009).

4.3.4. Diatom-related biomarkers
The concentration of 24-norcholestane (ααα C_{26} sterane), a possible biomarker for diatoms (Holba et al., 1998), is significant (avg.: 2.68 µg/g TOC). C_{25} HBI alkanes and thiophenes are also biomarkers indicating diatoms (Yon et

Table 1. Bulk parameters for Ruslar Formation.

	Sample no.	Height	S1	S2	Tmax	TOC	S	PI	HI	TOC/S	Calc. equiv.
		[m]	[mg HC/g rock]		[°C]	[%]	[%]	[-]	[mg HC/g TOC]	[-]	[%]
Karadere	29	14.5	0.05	0.59	422	0.96	0.34	0.08	61	2.80	1.70
	28	14.0	0.09	1.08	426	0.98	0.10	0.07	110	9.59	3.65
	27	13.5	0.10	2.42	426	1.76	1.50	0.04	137	1.17	6.53
	26	13.0	0.14	4.58	427	2.04	1.50	0.03	224	1.36	6.60
	25	12.5	0.18	5.54	427	2.17	1.10	0.03	256	1.96	5.42
	24	12.0	0.15	5.00	425	1.88	1.45	0.03	266	1.29	9.55
	23	11.5	0.14	4.73	423	1.93	0.80	0.03	246	2.40	6.65
	22	11.0	0.11	5.19	423	1.99	1.32	0.02	261	1.50	5.91
	21	10.5	0.11	5.91	422	2.04	1.35	0.02	289	1.52	7.79
	20	10.0	0.11	4.35	425	1.83	1.66	0.02	238	1.10	6.29
	19	9.5	0.12	6.22	422	2.24	1.42	0.02	278	1.58	6.68
	18	9.0	0.13	5.19	423	2.10	1.38	0.02	247	1.52	6.46
	17	8.5	0.13	4.61	421	1.88	1.39	0.03	245	1.35	5.91
	16	8.0	0.14	5.03	421	1.85	1.31	0.03	272	1.41	4.42
	15	7.5	0.13	5.20	421	2.19	0.60	0.02	237	3.66	5.89
	14	7.0	0.16	5.85	419	2.31	0.56	0.03	253	4.13	6.70
	13	6.5	0.12	6.35	422	2.30	1.32	0.02	276	1.74	7.25
	12	6.0	0.12	5.90	421	2.18	1.26	0.02	271	1.73	8.19
	11	5.5	0.14	5.20	420	2.03	1.49	0.03	256	1.37	8.76
	10	5.0	0.13	4.71	421	1.76	2.90	0.03	267	0.61	6.99
	9	4.5	0.14	4.11	429	1.67	1.40	0.03	246	1.19	10.48
	8	4.0	0.14	4.96	428	1.89	1.44	0.03	262	1.32	9.73
	7	3.5	0.15	5.69	426	2.16	1.49	0.03	263	1.45	6.20
	6	3.0	0.10	2.71	427	1.30	1.13	0.03	208	1.16	4.15
	5	2.5	0.07	0.84	436	0.82	1.35	0.08	102	0.60	6.75
	4	2.0	0.11	2.39	433	1.37	0.59	0.04	175	2.31	8.26
	3	1.5	0.08	1.48	430	1.03	1.50	0.05	143	0.69	5.50
	2	1.0	0.17	6.58	426	2.48	1.24	0.02	265	2.01	5.92
	1	0.5	0.22	8.48	424	2.56	1.39	0.02	331	1.84	8.50
P-79	1	350	0.27	1.6	415	1.40	1.15	0.1	102	1.3	2.00
	2	360	0.30	1.7	417	1.88	0.91	0.2	107	1.7	2.92
	3	370	0.25	1.6	422	1.26	0.72	0.1	100	2.2	1.75
	4	380	0.42	3.3	427	1.95	1.13	0.1	210	1.4	5.25
	5	400	0.56	4.7	427	1.43	1.43	0.1	300	1.1	11.58
	6	410	0.37	3.6	423	1.6	1.11	0.1	229	1.4	11.33

TOC - Total organic carbon, S - sulfur, HI - hydrogen index, PI - production index, calc. equi. - calcite equivalent.
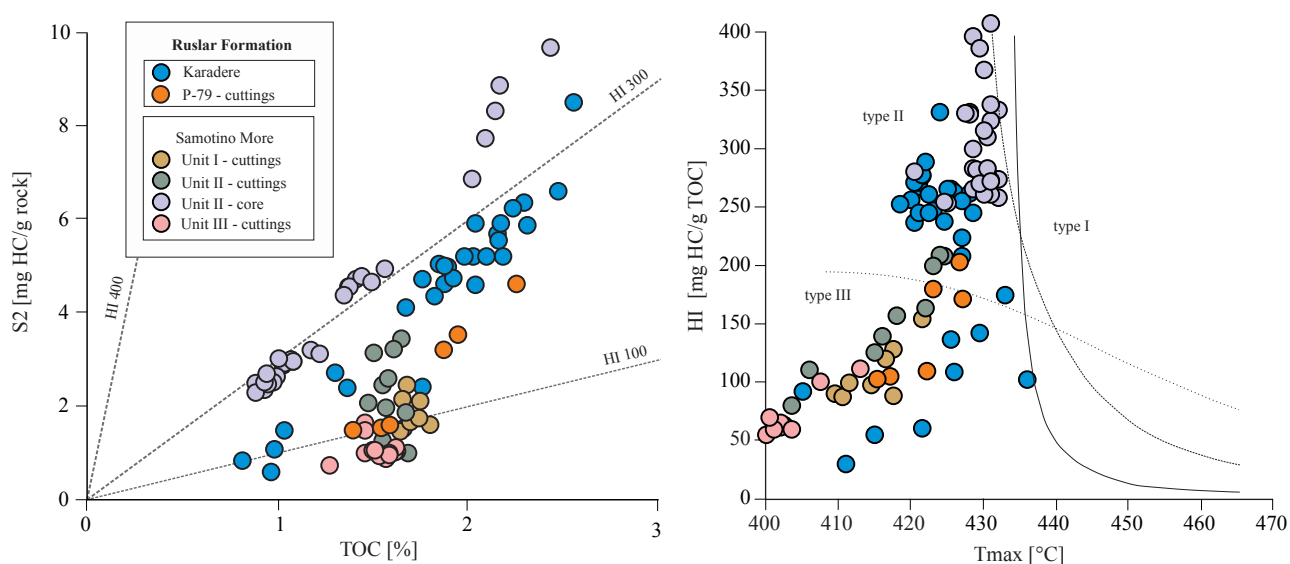
Figure 6. S2 vs. TOC hydrogen index (HI) vs. Tmax plots for the Ruslar Formation (Ruslar Formation at Karadere and Shkorpilovtsi P-79 relative to the offshore Ruslar Formation data from Samotino More wells from Sachsenhofer et al., 2009). The Ruslar Formation contains type II and III kerogen.

Table 2. Organic geochemical data of the Ruslar Formation at Karadere.

Sample no.	Height	TOC	HI	EOM	HC	NSO	Asph.	n-C_{15-19}	n-C_{21-25}	n-C_{26-31}	Steroids/ hopanoids	Hop-17 (21)-ene	28,30- Bisnorhopane	ααα C26 sterane	C_{25} HBI	Pr/Ph	MPI index
	[m]	[wt.%]	[mg/g TOC]	[%]							[μg/g TOC]						
28	14.5	0.98	97	39.0	14	34	52	29	27.1	44.6	9.9	1.2	53.7	9.8	9.6	1.0	0.9
25	12.5	2.17	271	21.0	15	71	14	45	24.0	32.7	7.1	0.2	0.3	4.0	9.0	0.8	1.0
22	11.0	1.99	261	19.5	12	72	16	29	25.3	47.0	5.4	0.8	12.6	2.8	8.8	0.8	0.9
19	9.5	2.24	278	17.9	17	74	8	19	28.8	52.6	6.3	0.0	2.4	0.6	5.6	0.7	1.0
16	8.0	1.85	272	25.8	19	71	9	35	23.9	42.4	4.6	0.9	34.5	2.6	13.9	1.1	1.0
14	7.0	2.31	253	20.4	16	76	8	20	27.6	53.3	4.4	0.4	40.6	2.5	13.8	1.3	1.0
12	6.0	2.18	271	15.3	16	71	13	25	24.4	51.5	3.0	0.3	16.5	0.7	7.7	0.8	1.0
9	4.5	1.67	246	17.3	11	72	17	51	18.1	30.8	8.4	0.1	8.9	0.9	3.4	0.8	1.0
7	3.5	2.16	263	17.9	11	73	16	38	21.8	41.0	9.0	0.2	7.7	2.0	5.6	0.7	1.0
4	2.0	1.37	175	32.8	11	75	14	31	28.2	43.4	4.2	0.6	29.8	2.7	13.6	0.9	1.0
1	0.5	2.56	331	9.0	14	62	24	22	26.7	52.6	5.3	0.1	6.3	0.9	2.1	0.7	0.9

TOC - Total organic carbon, HI - hydrogen index, EOM - extracted organic matter, HC - hydrocarbons yields, NSO - polar compounds, Asph. - asphalthene, n-C_{15-19} - short-chain alkanes, n-C_{21-25} - medium-chain alkanes, n-C_{26-32} - long-chain alkanes; Pr/Ph - pristane/ phytane ratio.

al., 1982; Nichols et al., 1998; Kenig et al., 1990; Volkman et al., 1994). Their concentrations are on average 8.46 μg/g TOC. High values (13–14 μg/g TOC) are seen in samples 4 (2.0 m), 14 (7.0 m), and 16 (8.0 m).

4.3.5. Land-plant-related biomarkers
Aromatic triterpenoids (including oleanane/ursane types), indicative for the input of angiosperms (Bechtel et al., 2008

and references therein) occur in significant concentrations (up to 6.6 μg/g TOC). In contrast, diterpenoids, indicative for gymnosperms (Simoneit et al., 1986), have not been detected.

Perylene occurs in high amounts (19.7 μg/g TOC). It may have different precursors including fungi (Marynowski et al., 2013 and references therein).

4.4. Diatom assemblages

The positions of the samples selected for the quantification of diatom assemblages are shown in Figure 4. The diatom assemblages are remarkably well preserved with abundant and identifiable diatom valves. The diatoms are present in nine samples, whereas samples 18 (9.0 m), 22 (11.0 m), and 27 (13.5 m) yielded less than 150 counts/sample.

The diatom genera found in the Ruslar Formation at Karadere are shown in Plates I–III. Overall, 23 genera were recorded. Since Paleogene diatom assemblages of the WBSB are poorly understood, the diatom identifications presented here are down to the genus level and only a few species-level identifications are given.

The most frequent genera are *Paralia* (avg. 29%), *Distephanosira* (avg. 16%), and *Stephanopyxis* (avg. 15%). Common genera include *Coscinodiscus* (avg. 9%), *Hemiaulus*, *Pseudopodosira*, *Rouxia*, and *Xanthiopyxis*. The less abundant genera include *Actinoptychus*, *Azpeitia*, *Asterolampra*, *Delphineis*, *Diploneis*, *Distephanosira*, *Eunotogramma*, *Eurossia*, *Liradiscus*, *Lyrella*, *Plagiogramma*, *Pseudopodosira*, *Pseudotriceratium*, *Radialiplicata*, *Rouxia*, *Rutilaria*, *Saeptifera*, and *Triceratium* (<3% avg. each).

A distinct up-section change has been observed in the generic composition of the diatom assemblages (Figure 7). For instance, *Paralia* shows an up-section increase in abundance, reaching a peak (44%) in sample 25 (12.5 m). Furthermore, *Distephanosira* (Plate I, figs. 1–3) decreases in abundance up-section. *Stephanopyxis* is represented by a number of species (Plate I, figs. 7–14) and shows some cyclic variations with a maximum percentage of 20% (Plate I, fig. 7). *Coscinodiscus* is extremely diverse (Plate I, figs. 15–23; Plate II, figs. 15–16). An up-section decrease has been observed for *Coscinodiscus*, *Hemiaulus* and the fossil resting spore genus *Xanthiopyxis* (Plate I, fig. 7). *Hemiaulus* and *Xanthiopyxis* are present in most of the samples, except sample 27 (13.5 m) and sample 12 (6.0 m), respectively. Raphid pennates are present with a significantly lower abundance, and they are represented by genus *Lyrella*. Araphid pennates are represented by rare *Rhaphoneis*.

4.5. Silicoflagellate assemblage

Silicoflagellates are present in the Ruslar Formation at Karadere, but they are less common than diatoms. Four taxa were recorded: *Bachmannocena apiculata*, *Naviculopsis biapiculata*, *Distephanopsis crux*, and *Corbisema regina* (Plate IV). In addition to silicoflagellates, we observed abundant synurophyte scales. *Macrora* is present in all samples, but is most frequent in samples 1 (0.5 m), 6 (3.0 m), and 9 (4.5 m), followed by *Corbisema regina*? and *Bachmannocena apiculata*?. *Naviculopsis biapiculata*? has been observed in only two samples: 3 (1.5 m) and 9 (4.5 m).

4.6. Calcareous nannofossils

The investigated samples generally contain similar exceptionally well-preserved and common calcareous nannofossil assemblages characterized by very low diversity (7–15 species). All samples are dominated by reticulofenestrids, predominately by *Reticulofenestra dictyoda* followed by *Reticulofenestra lockeri* and *Reticulofenestra minuta*. *Coccolithus pelagicus*, *Cyclicargolithus floridanus*, *Coronocyclus nitescens*, *Dictyococcites bisectus*, *Dictyococcites hesslandii*, and *Umbilicosphaera jafari* regularly occur. Helicoliths are represented by *Helicosphaera recta* and *Helicosphaera perch-nielseniae*. Among muroliths, *Pontosphaera versa* and *Pontosphaera multipora* regularly occur. Rare sphenoliths represented by *Sphenolithus moriformis* could be observed only in sample 1 (0.5 m). Discoasters are absent in all samples. Reworking from older sediments is very rare and presented by Upper Cretaceous species *Tetrapodorhabdus decorus* and *Watznaueria barnesiae*.

5. Discussion

5.1. Maturity and hydrocarbon source rock potential

Tmax values of the Ruslar Formation (avg. 424 °C) indicate that the Karadere section is immature. This statement is supported by the presence of hop-17(21)-enes (Luo et al., 2012). Whereas TOC contents classify the Ruslar Formation as good to very good source rocks (Figure 8), the petroleum potential suggests a fair to good quality. This discrepancy results from the presence of type II–III kerogen with relatively low hydrogen contents (avg. HI: 231 mgHC/gTOC) (Figure 6). Thus, the samples could generate gas, condensate, and oil.

Cuttings samples from borehole P-79 and unit I and III samples from Samotino More (Sachsenhofer et al., 2009) have an even lower petroleum potential, while unit II samples (NP23) have comparable potential (Figure 8).

The source potential index (SPI = thickness × (S1 + S2) × bulk density / 1000; Demaison and Huizinga, 1994) gives an indication of the amount of hydrocarbons (in tons HC) that can be generated beneath 1 m^2 of surface area. For the calculation, the net mudstone thickness has been estimated as 15 m because of the low percentage of sandstone layers. Taking into account the shallow burial depth and the high amount of diatoms, a density of only 2.0 g/cm^3 has been applied. Considering an average S1 of 0.12 mg HC/g rock and an average S2 of 4.51 mg HC/g rock, the SPI for the exposed part of the Ruslar Formation at Karadere is calculated as 0.14 t HC/m^2. Assuming that the measured values are representative for the entire Ruslar Formation and that the net mudstone thickness is 55 m, the SPI increases to 0.5 t HC/m^2, which is slightly lower than that in the Ruslar Formation of offshore Bulgaria (Sachsenhofer et al., 2018a, 2018b).
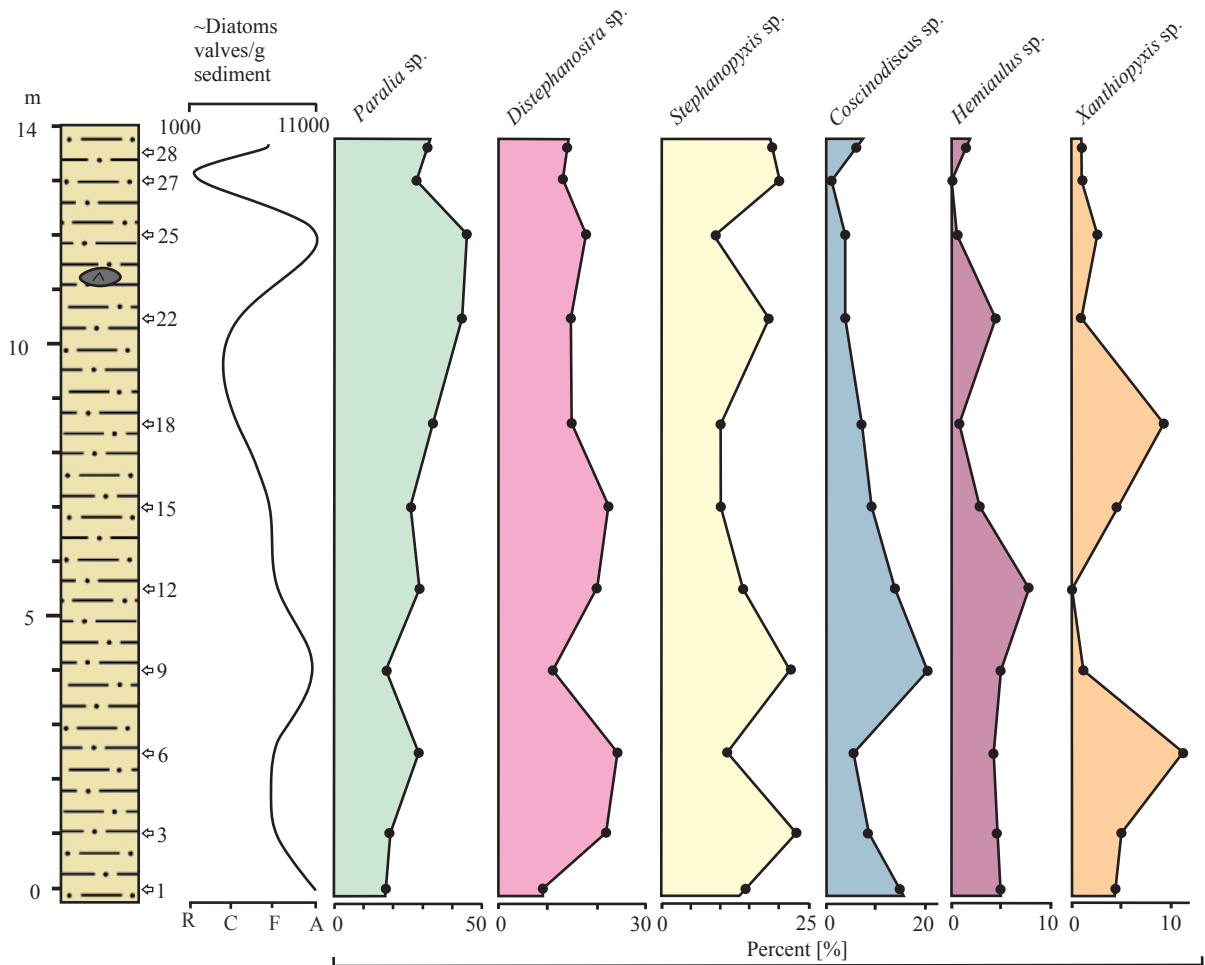
Figure 7. Variation in the relative abundance of the prevalent diatom genera with outcrop height observed at Karadere. R - rare, C - common, F - frequent, A - abundant.

5.2. Age and depositional environment

Diatom data are insufficient to provide an independent age control for the study site. Hence, the age of the Ruslar Formation at Karadere is entirely relying on calcareous nannofossils. Samples contain *Pontosphaera versa*, which has its last occurrence (top) within NP23 (Bown, 2005), accompanied by *Helicosphaera recta* and *Helicosphaera perch-nielseniae*, which both have their first occurrence within NP22 (de Kaenel and Villa, 1996; Boesiger et al., 2017). Based on the absence of *Reticulofenestra umbilicus*, all samples are attributed to the Early Oligocene standard nannoplankton zone NP23 (*Sphenolithus predistentus* zone) of Martini (1971). This assignment is further supported by the absence of *Sphenolithus ciperoensis*, the first occurrence of which defines the NP23/NP24 boundary, and nannofossil species that typically occur in zones NP24–NP25. The absence of discoasters and low diversity assemblages indicate shallow marine conditions. This interpretation is supported by the common

occurrence of small reticulofenestrids represented by *R. minuta* accompanied by helicoliths and muroliths, which points to the nearshore environment.

Diatoms occur in high abundance in the analyzed samples and provide important insights on the depositional environment. Although most of the interpretation is based on the present-day diatom environmental preferences, the interpretation should be treated as tentative, since diatom living preferences may change through time. For example, the modern *Paralia* is a tychopelagic species common in the North Sea (Gebühr et al., 2009) and can be found in both the plankton and benthos of modern temperate coastal environments (McQuoid and Nordberg, 2003). The extant *Paralia* is commonly associated with high primary productivity in coastal upwelling zones and strong physical mixing may play a crucial role in transporting cells into the plankton (e.g., Davies and Kemp, 2016). *Paralia* was found to be a common constituent of pelagic/hemipelagic deposits, such as the Cretaceous Marca Shale (Davies and
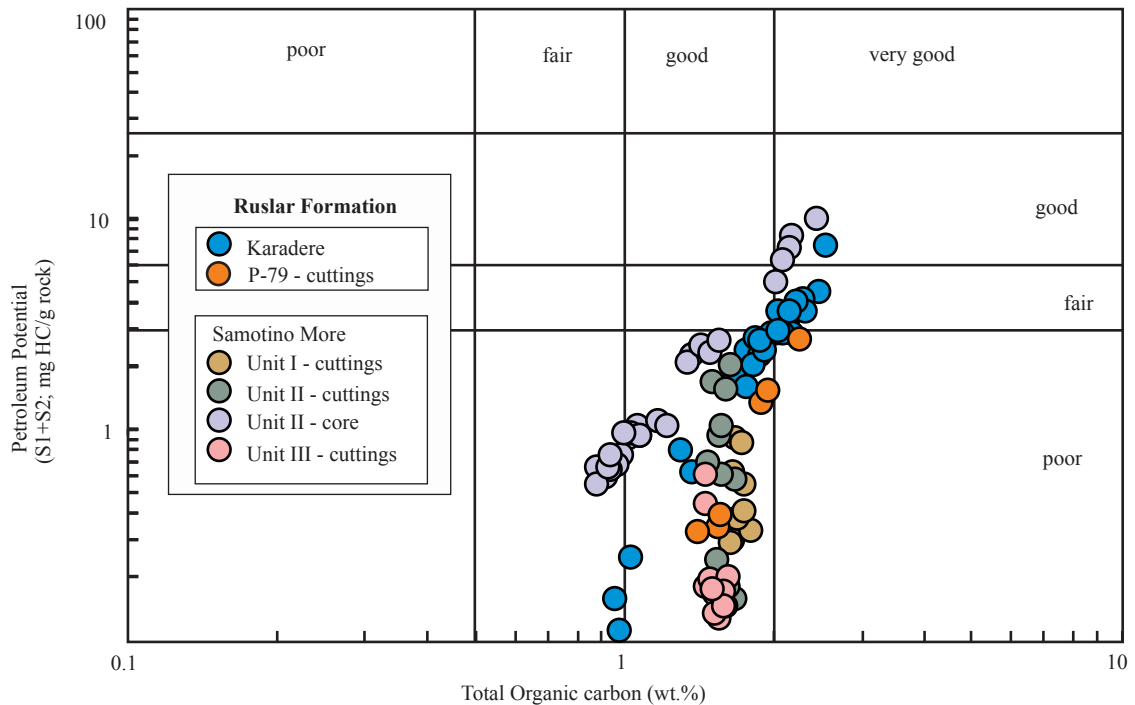
Figure 8. Petroleum potential of the Ruslar Formation at Karadere versus the Ruslar Formation offshore (Samotino More well data from Sachsenhofer et al., 2009 and Shkorpilovtsi P-79).

Kemp, 2016). A global distribution has been observed for *Distephanosira*, especially *D. architecturalis*, which was described from costal, neritic, and pelagic middle Eocene to late Oligocene successions (Witkowski et al., 2014). *Stephanopyxis* is a common planktonic genus. In the modern oceans it is found in regions of tropical or warm waters (Round et al., 1990). It is also adapted to live in a stratified water column and is capable of reproducing at rapid rates in low light conditions (Goldman, 1993; Kemp et al., 2006). Another planktonic diatom adapted to stratified waters, and often considered an indicator of oligotrophic conditions, is *Hemiaulus* (Kemp et al., 2006). The stratified-adapted species like *Stephanopyxis* and *Hemiaulus* are able to rapidly reproduce in conventional blooms, but they can also gradually accumulate in deep chlorophyll maxima (Kemp et al., 2006).

Xanthiopyxis is a fossil resting spore morphogenus associated with the marine diatom genus *Chaetoceros* (Suto, 2004). When nutrient levels are depleted, many diatom species form thick-walled resting spores that sink to deeper levels or to the sea floor and wait for more favorable conditions for vegetative growth (Suto, 2004). High abundance of *Xanthiopyxis* in at least two intervals in the studied succession likely points to a pronounced seasonality in nutrient levels during these periods.

In the Ruslar Formation at Karadere, *Stephanopyxis* abundance shows a series of fluctuations that generally parallel the percentage of *Hemiaulus*, which is generally low (<8%). *Xanthiopyxis* displays an opposite trend (Figure 7). This may indicate that a water column stratification developed periodically, with intermittent periods of pronounced seasonality in nutrient supply, perhaps linked to invigorated vertical mixing.

Water column stratification resulted in oxygen-depleted bottom water conditions, which are indicated by low Pr/Ph ratios and the presence of hop-17(21)-ene (Luo et al., 2012). Considering the high amount of diatoms, the presence of diatom-related biomarkers (24-norcholestane; C_{25}HBI alkanes and thiophenes) is not surprising. The presence of 28,30-bisnorhopane may indicate upwelling (e.g., Watson et al., 2009). However, bisnorhopane occurs in significant amounts in various anoxic settings (e.g., Pedersen et al., 2006). Moreover, upwelling is not supported by the observed calcareous nannofossil assemblages. These assemblages are characterized by high amounts of reticulofenestrids, whereas *Coccolithus pelagicus* occurs in very low amounts in all investigated samples. Assemblages with high amounts of *C. pelagicus* indicate marine environments with higher nutrient levels caused by upwelling conditions (Okada and McIntyre, 1979; Winter et al., 1994). In contrast to *C. pelagicus*, common occurrences of small reticulofenestrids among nannofossil assemblages indicate a shallow, well-stratified water column (Perch-Nielsen, 1985). Wade and Bown (2006)

165

observed the cooccurrence of diatoms and abundant *Reticulofenestra minuta* in extreme paleoenvironments during the Messinian salinity crises in the Polemi Basin (Cyprus) and concluded that this species tolerates brackish to hypersaline environments. Abundant *R. minuta* in low diversity assemblages occurs there before and after the deposition of evaporates (Wade and Bown, 2006) caused by basin isolation. In analogy, the low diversity calcareous nannofossil assemblages accompanied by diatoms may point to sedimentation after the "Solenovian event".

The detected calcareous nannoplankton assemblage and the abundance of plant debris agree with the postulated shallow marine environment. High amounts of terrestrial plants are also reflected by a relatively low HI and high amounts of C_{29} steroids. The presence of triterpenoids and the absence of diterpenoids show that the terrestrial input is dominated by angiosperms.

Overall, it is concluded that the studied section of the Lower Oligocene Ruslar Formation was deposited in a neritic marine environment, away from the wave zone. The surface water was mostly well oxygenated, but at least periodic water column stratification resulted in oxygen-depleted bottom water. Evidence for major changes in salinity could not be observed.

4.5. Regional understanding

As mentioned before, the Ruslar Formation typically contains from base to top calcareous shales (NP21–NP22), marlstones to limestone representing the low salinity Solenovian event (lower part of NP23), and overlying pelitic rocks with low carbonate contents (upper part of NP23 to NP24). Following the Solenovian event, the connection with the open ocean was partially restored during upper NP23 (Popov et al., 1993). Sachsenhofer et al. (2009) subdivided the Ruslar Formation of offshore Bulgaria into six units (from bottom to top: unit I to VI, whereby the diatom-rich unit VI turned out to be part of the Kaliakra canyon fill and should not be considered part of the Ruslar Formation; Mayer et al., 2018a). Their unit II corresponds to the NP23 (Solenovian event and overlying rocks).

The fragment of the Ruslar Formation exposed at Karadere was deposited in a fully marine environment and probably represents the (marine) upper part of NP23 (upper part of unit II). Hence, it is assumed that the "Solenovian event" is hidden in the unexposed lower part of the Ruslar Formation.

Within this context, it is important to note that the "Solenovian event" is probably missing at Karaburun along the Turkish Black Sea coast (İhsaniye Formation, Simmons et al., 2020; Tulan et al., 2020), located about 185 km SSE of Karadere. This may indicate that a connection between the Paratethys and the Mediterranean Sea remained open at the southwestern edge of the Black Sea.

The top of the Ruslar Formation in the Karadere area is formed by an erosional unconformity, and the uppermost part of the Ruslar Formation has been eroded. We speculate that the erosion is related to the incision of the Kaliakra canyon of offshore Bulgaria, which has been described in detail by Mayer et al. (2018a). This implies that the base of the Galata Formation may be considered as part of the canyon fill.

6. Conclusions and outlook

The fragment of the Ruslar Formation outcropping at Karadere along the western Black Sea shore exposes organic-rich, diatom-rich mudstones with sandstone intercalations, about 15 m thick, which have been dated as intra-Early Oligocene (biozone NP23). The lower part of the Ruslar Formation (including the "Solenovian event") is not exposed. Stratigraphically higher parts have been removed by erosion.

The mudstones are characterized by well-preserved diatom-rich assemblages, which are unique for sediments of this age in the Black Sea area. Diatom assemblages, frequent silicoflagellate skeletons, and calcareous nannoplankton and rare foraminifera suggest a fully marine, neritic environment. Whereas the surface water was oxygenated, water column stratification caused oxygen-depleted bottom water conditions. Apart from oxygen depletion, biomarker data also provide evidence for strong input of terrestrial organic matter, dominated by angiosperms. Not surprisingly, diatom-related biomarkers occur in significant concentrations.

The hydrocarbon potential of the Oligocene rocks is fair to good, with an average TOC of 1.85% wt. and type II–III kerogen (avg. HI: 231 mg HC/g TOC), which may generate oil and gas. The organic matter is thermally immature. The SPI shows that the exposed section may generate about 0.2 t HC/m² when mature. A rough estimate of the SPI for the entire Ruslar Formation at Karadere (including the nonexposed part) is 0.5 t HC/m². This value is low, but in the order of other Oligocene sections of offshore Bulgaria.

To our knowledge, this paper provides the first detailed description of diatoms in the Ruslar Formation. To study variations of the depositional environment, we suggest investigating diatoms from the Ruslar Formation (and the Miocene fill of the Kaliakra canyon) in additional locations. Furthermore, the investigation of the lower part of the Ruslar Formation in onshore locations, which is currently not accessible in the field, is highly recommended in order to determine changes in depositional environment and hydrocarbon potential.

References

Aladzova-Hrisceva K (1991). Stratigraphy, subdivision and correlation of Paleogene deposits in northeastern Bulgaria. Geologica Balkanica 21: 12-28 (in Russian).

Báldi T (1984). The terminal Eocene and Early Oligocene events in Hungary and the separation of an anoxic, cold Paratethys. Eclogae Geologicae Helvetiae 77 (1): 1-27.

Bechtel A, Gratzer R, Sachsenhofer RF, Gusterhuber J, Lücke A et al. (2008). Biomarker and carbon isotope variation in coal and fossil wood of Central Europe through the Cenozoic. Palaeogeography, Palaeoclimatology, Palaeoecology 262 (3-4): 166-175. doi: 10.1016/j.palaeo.2008.03.005

Bechtel A, Markic M, Sachsenhofer RF, Jelen B, Gratzer R et al (2004). Paleoenvironment of the Upper Oligocene Trbovlje coal seam (Slovenia). International Journal of Coal Geology 57 (1): 23-48. doi: 10.1016/j.coal.2003.08.005

Bechtel A, Sachsenhofer RF, Kolcon I, Gratzer R, Otto A et al. (2002). Organic geochemistry of the Lower Miocene Oberdorf lignite (Styrian Basin, Austria): Its relation to petrography, palynology and the palaeoenvironment. International Journal of Coal Geology 51 (1): 31-57. doi: 10.1016/s0166-5162(02)00079-4

Bechtel A, Widera M, Sachsenhofer RF, Gratzer R, Lücke A et al. (2007). Biomarker and stable carbon isotope systematics of fossil wood from the second Lusatian lignite seam of the Lubstow deposit (Poland). Organic Geochemistry 38 (11): 1850-1864. doi: 10.1016/j.orggeochem.2007.06.018

Boesiger TM, de Kaenel E, Bergen JA, Browning E, Blair SA (2017). Oligocene to Pleistocene taxonomy and stratigraphy of the genus *Helicosphaera* and other placolith taxa in the circum North Atlantic Basin. Journal of Nannoplankton Research 37 (2-3): 145-175.

Bown PR (2005). Palaeogene calcareous nannofossils from the Kilwa and Lindi areas of coastal Tanzania (Tanzania Drilling Project 2003-4). Journal of Nannoplankton Research 27 (1): 21-95.

Cheshitev G, Kancev I (1989). Geological map of People`s Republic of Bulgaria. 1:500.000. Sofia, Bulgaria: Committee of Geology, Department of Geophysical Prospecting and Geological Mapping.

Dachev C, Stanev V, Bokov P (1988). Structure of the Bulgarian Black Sea area. Bullettino di Geofisica Teorica ed Applicata 30: 79-107.

Davies A, Kemp AES (2016). Late Cretaceous seasonal palaeoclimatology and diatom palaeoecology from laminated sediments. Cretaceous Research 65: 82-111. doi: 10.1016/j.cretres.2016.04.014

de Kaenel E, Villa G (1996). Oligocene-Miocene calcareous nannofossil biostratigraphy and paleoecology from the Iberian Abyssal Plain. Proceedings of the Ocean Drilling Program, Scientific Results 149: 79-145. doi: 10.2973/odp.proc.sr.149.208.1996

Demaison G, Huizinga BJ (1994). Genetic classification of petroleum systems using three factors: charge, migration and entrapment. AAPG Memoirs 60: 73-92.

Didyk BM, Simoneit BR, Brassell ST, Eglinton G (1978). Organic geochemical indicators of paleoenvironmental conditions of sedimentation. Nature 272 (5650): 216-222. doi: 10.1038/272216a0

Eglinton G, Hamilton RJ (1967). Leaf epicuticular waxes. Science 156 (3780): 1322-1335. doi: 10.1126/science.156.3780.1322

Ficken KJ, Li B, Swain DL, Eglinton G (2000). An n-alkane proxy for the sedimentary input of submerged/floating freshwater aquatic macrophytes. Organic Geochemistry 31 (7-8): 745-749. doi: 10.1016/s0146-6380(00)00081-4

Gebühr C, Wiltshire K, Aberle N, van Beusekom J, Gerdts G (2009). Influence of nutrients, temperature, light and salinity on the occurrence of *Paralia sulcata* at Helgoland Roads, North Sea. Aquatic Biology 7: 185-197. doi: 10.3354/ab00191

Georgiev G (2011). Geology and hydrocarbon systems in the Western Black Sea. Turkish Journal of Earth Sciences 21 (5): 723-754. doi: 10.3906/yer-1102-4

Georgiev G, Dabovski C (1997). Alpine structure and petroleum geology of Bulgaria. Geology and Mineral Resources 8/9, 3-7 (in Bulgarian). doi: 10.1306/3b05b0b0-172a-11d7-8645000102c1865d

Goldman JC (1993). Potential role of large oceanic diatoms in new primary production. Deep Sea Research Part I: Oceanographic Research Papers 40 (1): 159-168. doi: 10.1016/0967-0637(93)90059-c

Holba AG, Dzou LI, Masterson WD, Hughes WB, Huizinga BJ et al. (1998). Application of 24-norcholestanes for constraining source age of petroleum. Organic Geochemistry 29 (5-7): 1269-1283. doi: 10.1016/s0146-6380(98)00184-3

Kemp AES, Pearce RB, Grigorov I, Rance J, Lange CB et al. (2006). Production of giant marine diatoms and their export at oceanic frontal zones: Implications for Si and C flux from stratified oceans. Global Biogeochemical Cycles 20 (4): 1-13. doi: 10.1029/2006gb002698

Kenig F, Huc AY, Purser BH, Oudin JL (1990). Sedimentation, distribution and diagenesis of organic matter in recent carbonate environment, Abu Dhabi, UAE. Organic Geochemistry 16 (4-6): 735-747. doi: 10.1016/0146-6380(90)90113-e

Lafargue E, Marquis F, Pillot D (1998). Rock-Eval 6 applications in hydrocarbon exploration, production, and soil contamination studies. Revue de l'Institut Français Du Pétrole 53 (4): 421-437. doi: 10.2516/ogst:1998036

Luo Q, Yu S, Liu Y, Zhang Y, Han H et al. (2012). Existence and implications of hop-17 (21)-enes in the lower cretaceous of the Saihantala Sag, Erlian Basin, China. Petroleum Science 9 (2): 154-160. doi: 10.1007/s12182-012-0195-8

Martini E (1971). Standard Tertiary and Quaternary calcareous nannoplankton zonation. In: Proceedings of the II Planktonic Conference. Rome, Italy: Tecnoscienza, pp. 739-785.

Marynowski L, Smolarek J, Bechtel A, Philippe M, Kurkiewicz S et al. (2013). Perylene as an indicator of conifer fossil wood degradation by wood-degrading fungi. Organic Geochemistry 59: 143-151. doi: 10.1016/j.orggeochem.2013.04.006

Mayer J, Rupprecht BJ, Sachsenhofer RF, Tari G, Bechtel A et al. (2018a). Source potential and depositional environment of Oligocene and Miocene rocks offshore Bulgaria. Geological Society of London Special Publications 464 (1): 307-328. doi: 10.1144/sp464.2

Mayer J, Sachsenhofer RF, Ungureanu C, Bechtel A, Gratzer R et al. (2018b). Petroleum charge and migration in the Black Sea: insights from oil and source rocks geochemistry. Journal of Petroleum Geology 41: 337-35. doi: 10.1111/jpg.12706

McQuoid M, Nordberg K (2003). The diatom *Paralia sulcata* as an environmental indicator species in coastal sediments. Estuarine, Coastal and Shelf Science 56 (2): 339-354. doi: 10.1016/s0272-7714(02)00187-7

Moldowan JM, Fago FJ (1986). Structure and significance of a novel rearranged monoaromatic steroid hydrocarbon in petroleum. Geochimica et Cosmochimica Acta 50 (3): 343-351. doi: 10.1016/0016-7037(86)90188-2

Nichols PD, Volkman JK, Palmisano AC, Smith GA, White DC (1988). Occurrence of an isoprenoid C25 diunsaturated alkene and high neutral lipid content in Antarctic sea-ice diatom communities. Journal of Phycology 24 (1): 90-96. doi: 10.1111/j.1529-8817.1988.tb04459.x

Nikishin AM, Okay AI, Tüysüz O, Demirer A, Amelin N et al. (2015). The Black Sea basins structure and history: New model based on new deep penetration regional seismic data. Part 1: Basins structure and fill. Marine and Petroleum Geology 59: 638-655. doi: 10.1016/j.marpetgeo.2014.08.017

Noble R, Alexander R, Kagi RI (1985). The occurrence of bisnorhopane, trisnorhopane and 25-norhopanes as free hydrocarbons in some Australian shales. Organic Geochemistry 8 (2): 171-176. doi: 10.1016/0146-6380(85)90035-x

Okada H, McIntyre A (1979). Seasonal distribution of the modern Coccolithophores in the western North Atlantic Ocean. Marine Biology 54: 319-328.

Ourisson G, Albrecht P, Rohmer M (1979). The Hopanoids: palaeochemistry and biochemistry of a group of natural products. Pure and Applied Chemistry 51 (4): 709-729. doi: 10.1351/pac197951040709

Pedersen JH, Karlsen DA, Backer-Owe K, Lie JE, Brunstad H (2006). Two geochemistry of two unusual oils from the Norway North Sea: implications for new source rock and play scenario. Petroleum Geoscience 12: 85-96.

Perch-Nielsen K (1985). Cenozoic calcareous nannofossils. In: Bolli HM, Saunders JB, Perch-Nielsen K (editors). Plankton Stratigraphy. Cambridge, UK: Cambridge University Press, pp. 427-554.

Popov N, Kojumdjieva E (1987). The Miocene in northeastern Bulgaria (lithostratigraphic subdivision and geologic evolution). Review of the Bulgarian Geological Society 38: 15-33 (in Bulgarian).

Popov SV, Voronina AA, Gontscharova IA (1993). Stratigraphy and bivalves of the Oligocene-Lower Miocene of the Eastern Paratethys. Moscow, Russia: Paleontological Institute of the Russian Academy of Sciences (in Russian).

Radke M, Willsch H, Welte DH (1980). Preparative hydrocarbon group type determination by automated medium pressure liquid chromatography. Analytical Chemistry 52 (3): 406-411. doi: 10.1021/ac50053a009

Rögl F (1997). Palaeogeographic considerations for Mediterranean and Paratethys seaways (Oligocene to Miocene). Annalen des Naturhistorischen Museums in Wien. Serie A für Mineralogie und Petrographie, Geologie und Paläontologie, Anthropologie und Prähistorie 279-310.

Rusu A (1999). Rupelian mollusk fauna of Solenovian type found in Eastern Carpathians (Romania). Acta Palaeontologica Romaniae 2: 449-452.

Sachsenhofer RF, Popov SV, Bechtel A, Ćorić S, Francu J et al. (2018a). Oligocene and Lower Miocene source rocks in the Paratethys: Palaeogeographic and stratigraphic controls. In: Simmons M (editor). Petroleum Geology of the Black Sea. London, UK: Geological Society Special Publications, pp. 267-306. doi: 10.1144/sp464.1

Sachsenhofer RF, Popov SV, Ćorić S, Mayer J, Misch D et al. (2018b). Parathethyan petroleum source rocks: an overview. Journal of Petroleum Geology 41 (3): 219-245. doi: 10.1111/jpg.12702

Sachsenhofer RF, Stummer B, Georgiev G, Dellmour R, Bechtel A et al. (2009). Depositional environment and hydrocarbon source potential of the Oligocene Ruslar Formation (Kamchia Depression; western Black Sea). Marine and Petroleum Geology 26 (1): 57-84. doi: 10.1016/j.marpetgeo.2007.08.004

Schrader H, Gersonde R (1978). Diatoms and silicoflagellates. Utrecht Micropaleontological Bulletins 17: 129-176.

Schrader HJ (1973). Proposal for a standardized method of cleaning diatom-bearing deep-sea and land-exposed marine sediments. Nova Hedwigia Supplement 45: 403-409.

Schultz L (1964). Quantitative Interpretation of Mineralogical Composition from X-ray and Chemical Data for the Pierre Shale. U.S. Geological Survey Professional Paper 391-C. Reston, VA, USA: USGS. doi: 10.3133/pp391c

Schulz HM, Bechtel AC, Rainer TH, Sachsenhofer RF, Struck UL (2004). Paleoceanography of the Western Central Paratethys during early Oligocene nannoplankton Zone NP23 in the Austrian Molasse Basin. Geologica Carpathica 55 (4): 311-323.

Simmons M, Bidgood M, Connel P, Coric S, Okay A et al. (2020). Biostratigraphy and palaeoenvironments of the Oligocene succession (Ihsaniye Formation) at Karaburun (NW Turkey). Turkish Journal of Earth Sciences 29: 28-63.

Simoneit BR, Grimalt JO, Wang TG, Cox RE, Hatcher PG et al. (1986). Cyclic terpenoids of contemporary resinous plant detritus and of fossil woods, ambers and coals. Organic Geochemistry 10 (4-6): 877-889. doi: 10.1016/s0146-6380(86)80025-0

Sinclair HD, Juranov SG, Georgiev G, Byrne P, Mountney NP (1997). The Balkan thrust wedge and foreland basin of Eastern Bulgaria: structural and stratigraphic development. In: Robinson AG (editor). Regional and Petroleum Geology of the Black Sea and Surrounding Region. Tulsa, OK, USA: American Association of Petroleum Geologists, pp. 91-114.

Suttill HL (2009). Sedimentological evolution of the Emine and Kamchia Basins, Eastern Bulgaria. MPhil thesis, University of Edinburgh, Edinburgh, UK.

Suto I (2004). Fossil marine diatom resting spore morpho-genus Xanthiopyxis Ehrenberg in the North Pacific and Norwegian Sea. Paleontological Research 8 (4): 283-310. doi: 10.2517/prpsj.8.283

Tari GC, Simmons MD (2018). History of deepwater exploration in the Black Sea and an overview of deepwater petroleum play types. In: Simmons M (editor). Petroleum Geology of the Black Sea. London, UK: Geological Society Special Publications, pp. 439-475. doi: 10.1144/sp464.16

Ten Haven HL, De Leeuw JW, Schenk PA (1985). Organic geochemical studies of a Messinian evaporitic basin, northern Apennines (Italy). I: Hydrocarbon biomarkers for a hypersaline environment. Geochimica et Cosmochimica Acta 49 (10): 2181-2191. doi: 10.1016/0016-7037(85)90075-4

Tulan E, Sachsenhofer RF, Tari G, Flecker R, Fairbank V et al. (2020). Source rock potential and depositional environment of Lower Oligocene rocks in the Karaburun area, Turkey. Turkish Journal of Earth Sciences 29: 64-84.

Valchev B, Sachkov D, Juranov S (2018). 3D lithostratigraphic model of the Paleogene of the onshore part of the Moesian Platform (Northeast Bulgaria). Geologica Balcanica 47 (1): 23-36.

Volkman JK, Barnett SM, Dunstan GA, Jeffrey SW (1994). C25 and C30 highly branched isoprenoid alkenes in laboratory cultures of two marine diatoms. Organic Geochemistry 21 (3-4): 407-13. doi: 10.1016/0146-6380(94)90202-x

Voronina AA, Popov SV (1984). Solenovian horizon from Eastern Paratethys. Bulletin of the Academy of Sciences of the USSR Geologic Series 9: 41-53 (in Russian).

Wade BS, Bown PR (2006). Calcareous nannofossils in extreme environments: The Messinian Salinity Crisis. Polemi Basin, Cyprus. Palaeogeography, Palaeoclimatology, Palaeoecology 233: 271-286. doi: 10.1016/j.palaeo.2005.10.007

Watson JS, Jolley DW, Kelley SP (2009). High concentration of 28,30-bisnorhopane and 25,28,30-trisnorhopane at the PETM in the Faroe-Shetland basin. In: 24th International Meeting on Organic Geochemistry; 6–11 September 2009; Bremen, Germany.

Winter A, Jordan R, Roth P (1994). Biogeography of living Coccolithophores in ocean waters. In: Winter A, Siesser W (editors). Coccolithophores. Cambridge, UK: Cambridge University Press, pp. 13-37.

Witkowski J, Bohaty SM, Edgar KM, Harwood DM (2014). Rapid fluctuations in mid-latitude siliceous plankton production during the Middle Eocene Climatic Optimum (ODP Site 1051, western North Atlantic). Marine Micropaleontology 106: 110-129. doi: 10.1016/j.marmicro.2014.01.001

Yon DA, Maxwell JR, Ryback G (1982). 2,6,10-Trimethyl-7-(3-methylbutyl)-dodecane, a novel sedimentary biological marker compound. Chemischer Informationsdienst 13 (43). doi: 10.1002/chin.198243163

Zolitschka B (1998). Paläoklimatische Bedeutung laminierter Sedimente. Holzmaar (Eifel, Deutschland), Lake C2 (Nordwest-Territorien, Kanada) und Lago Grande di Monticchio (Basilicata, Italien). Berlin, Germany: Bornträger (in German).
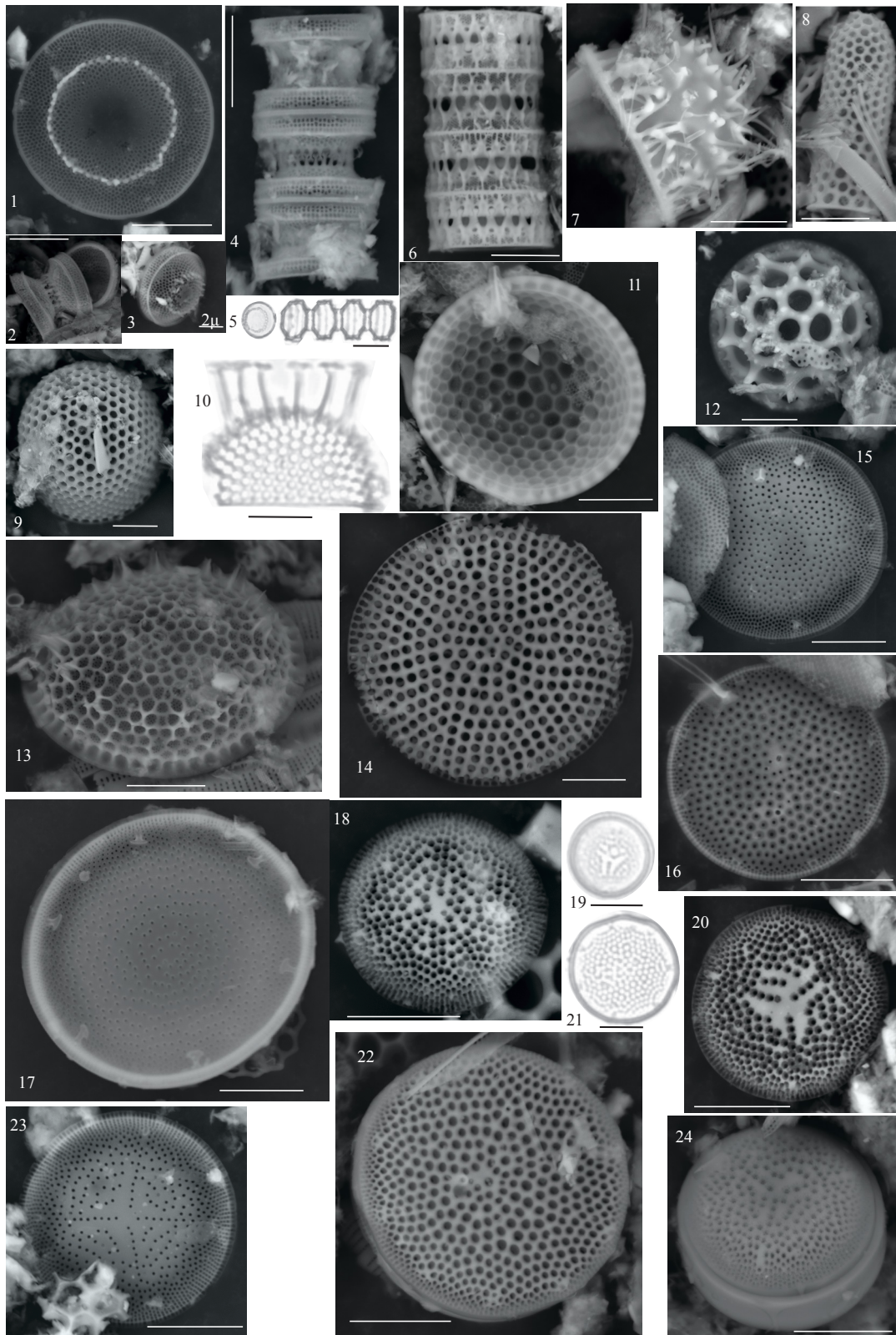
Plate I. Diatoms. **1–5:** *Distephanosira* sp.; fig. 5, view in LM of figs. 4 and 1. **6:** *Paralia* sp. **7:** Resting spore. **8–13:** *Stephanopyxis* spp. **14:** *Azpeitia* sp. **15:** *Actinocyclus*? sp. **16:** *Azpeitia* sp. **17–20:** *Coscinodiscus* spp.; fig. 19, LM view of fig. 18. **21–22:** *Azpeitia* sp.; fig., 21 LM view of fig. 22. **23-24:** *Coscinodiscus*? sp. *Scale bar is 10 μm unless specified otherwise. LM: light microscopy.
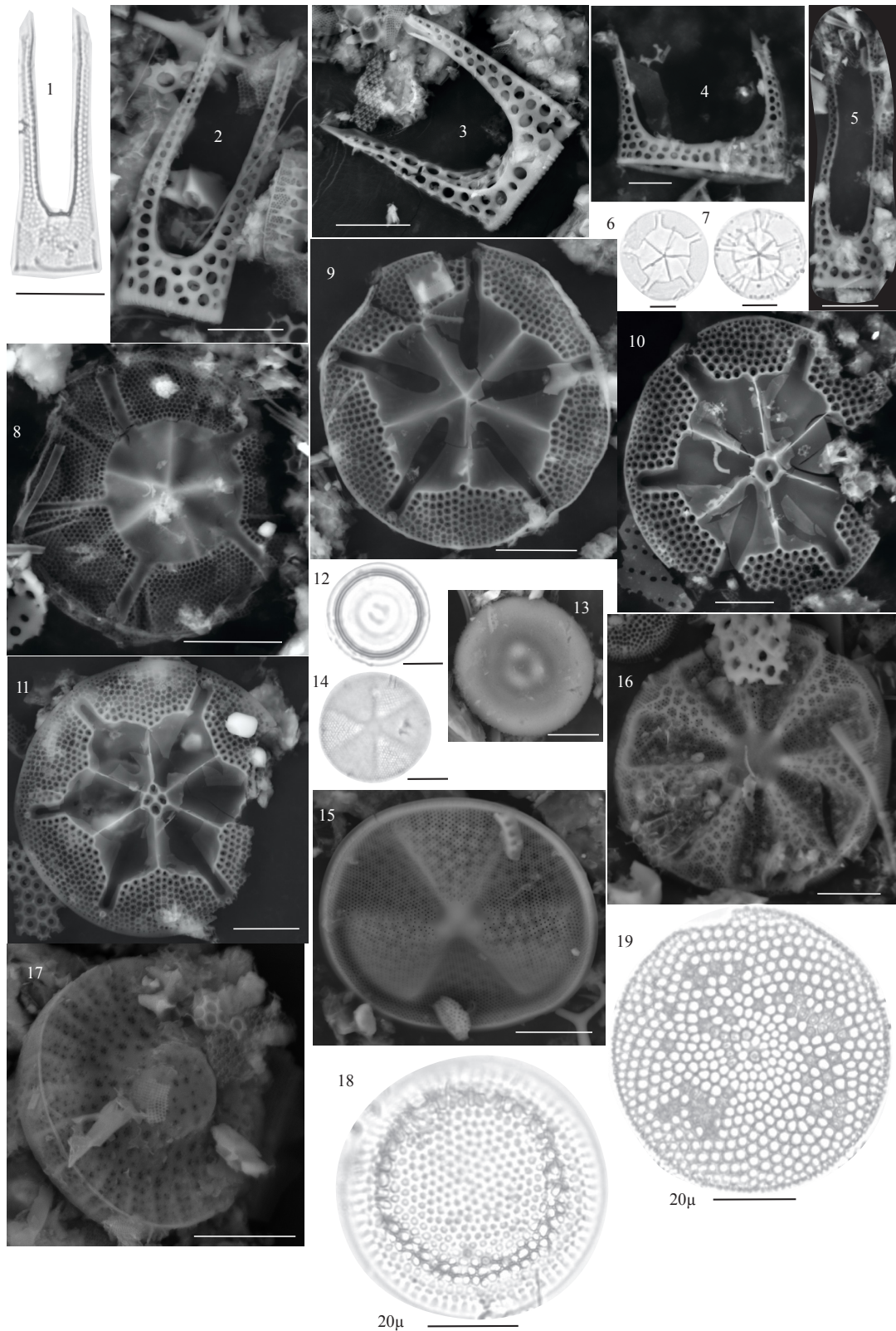
Plate II. Diatoms. **1–5:** *Hemiaulus* spp. **6–11:** *Asterolampra* spp. **12–13:** *Pseudopodosira* sp.; fig. 12, LM view of fig. 13. **14–15:** *Actinoptychus undulatus* (Bailey) Ralfs, in Pritchard (1861). **16:** *Actinoptychus* sp. cf. *A. maculatus* Grove and Sturt 1887. **17:** *Pseudostictodiscus?* sp. **18–19:** *Coscinodiscus?* *Scale bar is 10 μm unless specified otherwise. LM: light microscopy.
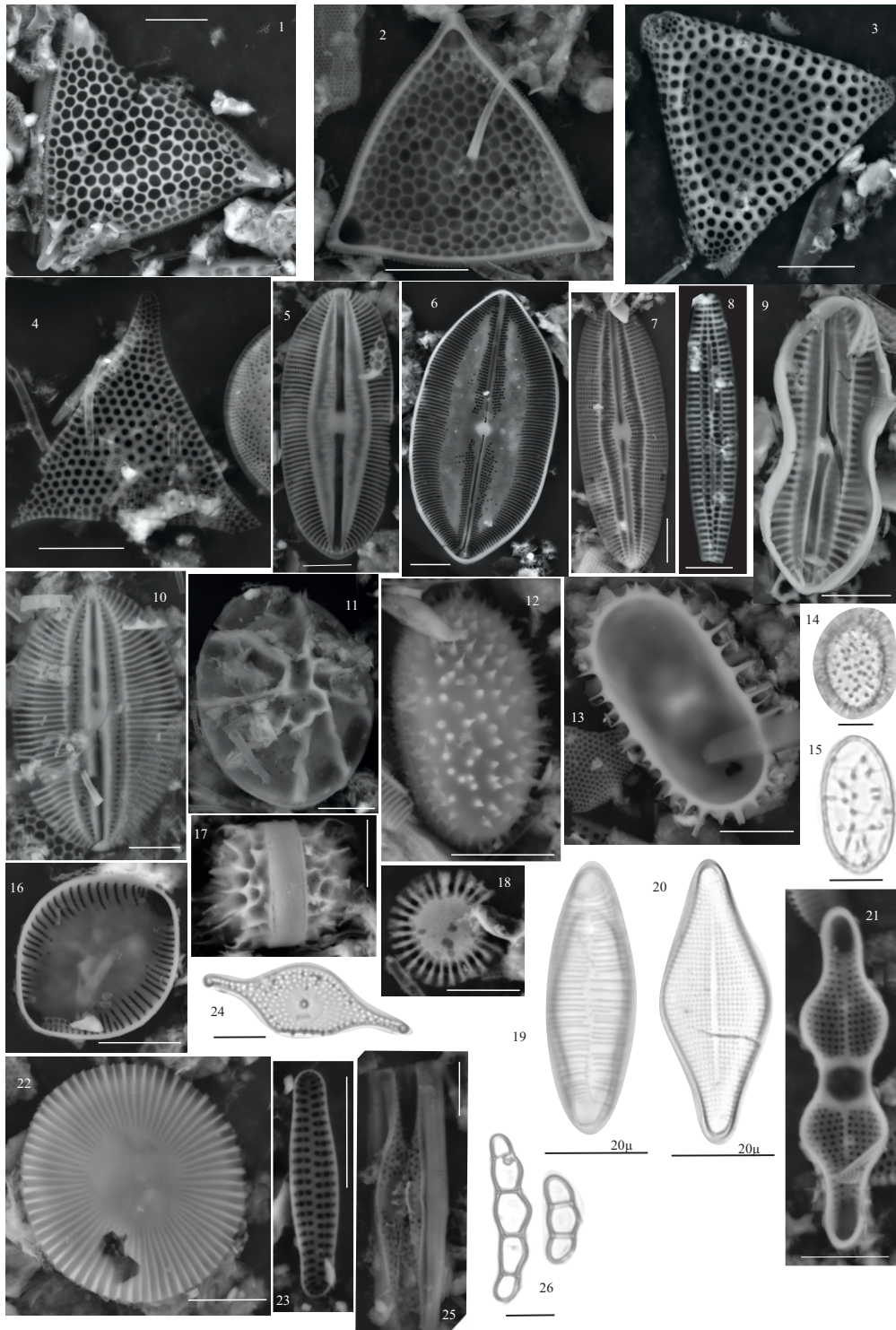
Plate III. Diatoms. **1–2:** *Triceratium* sp. cf. *T. dictyotum*? Sims and Ross (1990). **3:** *Eurossia irregularis* (Greville) P.A.Sims (1993). **4:** *Pseudotriceratium* Grunow (1884). **5–7:** *Lyrella* sp. **8:** *Rouxia* sp. (*Rouxia naviculoides*? Schrader). **9:** *Diploneis ornata?* Schmidt in Schmidt et al. (1881). **10:** *Lyrella*? sp. **11:** *Liradiscus*? sp. **12–13:** *Xanthiopyxis* sp. cf. *X. oblonga*. **14–15:** LM of *Xanthiopyxis* sp. **16:** Internal view of an unrecognizable pennate diatom. **17:** Unidentified resting spore of *Chaetoceros* sp. **18:** *Radialiplicata* sp. **19:** *Saeptifera* sp. **20:** *Delphineis surirella*? (Ehrenberg) G.W. Andrews (1981). **21:** *Plagiogramma* sp. **22:** *Radialiplicata* sp. **23:** Internal view of an unrecognizable diatom. **24:** *Rutilaria areolata* Sheshukova-Poretskaya in Sheshukova-Poretskaya and Gleser 1964. **25:** *Rutilaria* sp. cf. *R. attenuata* Ross 1990. **26:** *Eunotogramma* sp. *Scale bar is 10 μm unless specified otherwise. LM: light microscopy.
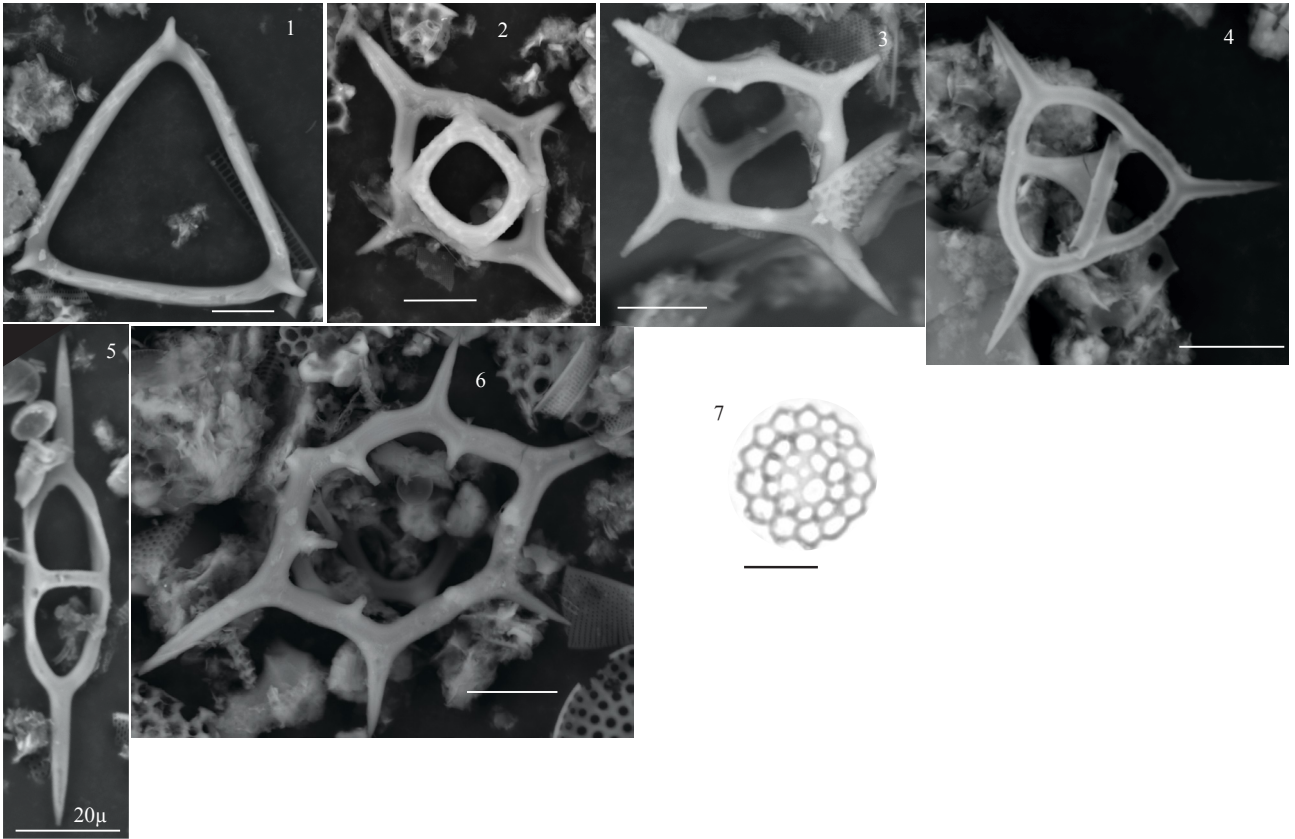
Plate IV. Silicoflagellates and other siliceous microfossils. **1:** *Bachmannocena* sp. (Locker, 1974) Burky (1987). **2–3:** *Distephanopsis crux* (Ehrenberg) P. Dumitrica. **4:** *Corbisema regina*? D. Burky. **5:** *Naviculopsis biapiculata* (Lemmermann) Frenguelli. **6:** *Stephanocha speculum* (Ehrenberg 1837) Jordan and McCartney 2015. **7:** *Macrora* sp. in LM. *Scale bar is 10 μm unless specified otherwise. LM: light microscopy.
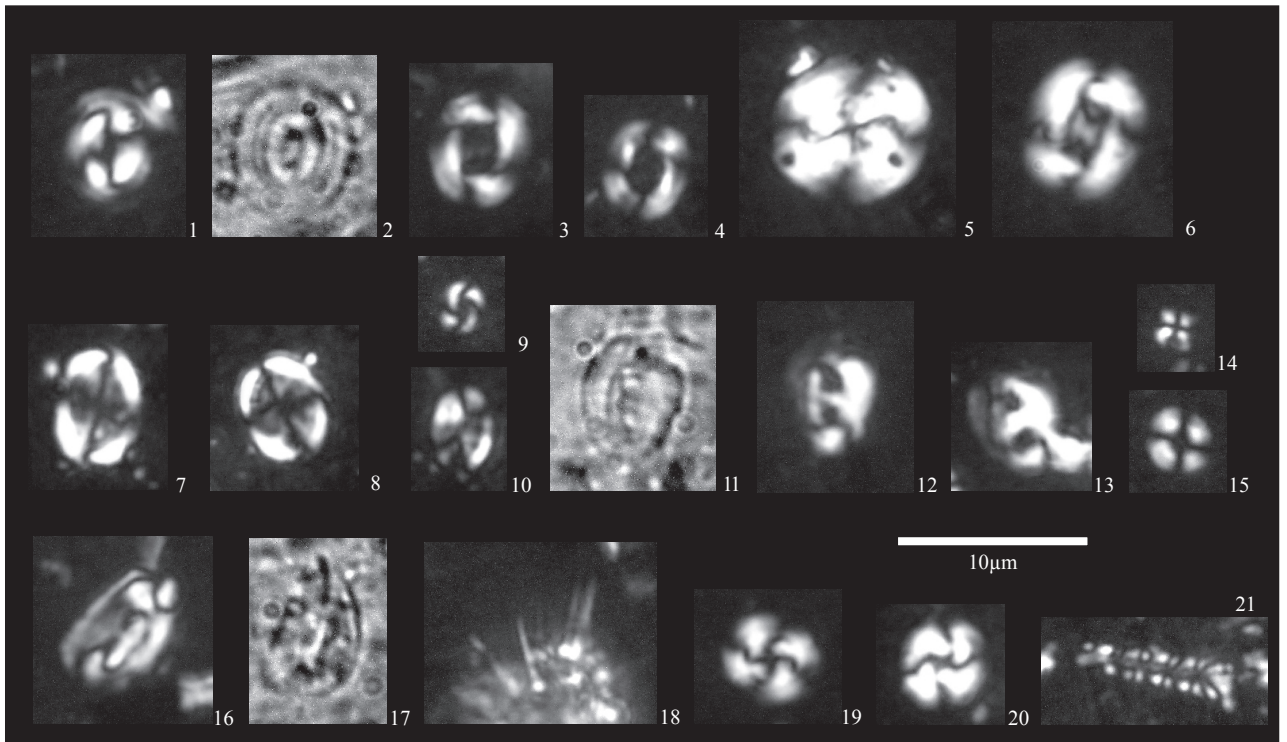
Plate V. Calcareous nannofossils. **1–2:** *Coccolithus pelagicus* (Wallich 1877) Schiller, 1930. **3–4:** *Reticulofenestra dictyoda* (Deflandre in Deflandre and Fert, 1954) Stradner in Stradner and Edwards, 1968. **5:** *Dictyococcites hesslandii* Haq 1971. **6:** *Reticulofenestra lockeri* Müller, 1970. **7–8:** *Pontosphaera versa* (Bramlette and Sullivan, 1961) Sherwood, 1974. **9:** *Reticulofenestra minuta* Roth, 1970. **10:** *Pontosphaera multipora* (Kamptner, 1948 ex Deflandre in Deflandre and Fert, 1954) Roth, 1970. **11–13:** *Helicosphaera recta* (Haq, 1966) Jafar and Martini, 1975. **14:** *Sphenolithus* sp. **15:** *Umbilicosphaera* cf. *jafari* Muller, 1974. **16–17:** *Helicosphaera perch-nielseniae* (Haq 1971) Jafar and Martini (1975). **18:** *Rhabdosphaera* sp. **19–20:** *Cyclicargolithus floridanus* (Roth and Hay, in Hay et al., 1967) Bukry, 1971. **21:** *Tetrapodorhabdus decorus* (Deflandre in Deflandre and Fert, 1954) Wind and Wise 1983**.**